Published in final edited form as:
Dev Biol. 2012 April 1; 364(1): 22–31. doi:10.1016/j.ydbio.2012.01.011.

An essential and highly conserved role for Zic3 in left-right patterning, gastrulation and convergent extension morphogenesis

Ashley E. Cast[a], **Chunlei Gao**[b], **Jeffrey D. Amack**[b], and **Stephanie M. Ware**[a,*]

[a]Division of Molecular Cardiovascular Biology, the Heart Institute, Department of Pediatrics, Cincinnati Children's Hospital Medical Center, 240 Albert Sabin Way, MLC 7020, Cincinnati, OH 45229-3039, USA

[b]Department of Cell and Developmental Biology, State University of New York Upstate Medical University, 750 E. Adams Street, Syracuse, NY 13210, USA

Abstract

Mutations in ZIC3 result in X-linked heterotaxy in humans, a syndrome consisting of left-right (L-R) patterning defects, midline abnormalities, and cardiac malformations. Similarly, loss of function of Zic3 in mouse results in abnormal L-R patterning and cardiac development. However, *Zic3* null mice also exhibit defects in gastrulation, neural tube closure, and axial patterning, suggesting the hypothesis that Zic3 is necessary for proper convergent extension (C-E) morphogenesis. To further investigate the role of Zic3 in early embryonic development, we utilized two model systems, *Xenopus laevis* and zebrafish, and performed loss of function analysis using antisense morpholino-mediated gene knockdown. Both *Xenopus* and zebrafish demonstrated significant impairment of C-E in Zic3 morphants. L-R patterning was also disrupted, indicating that the role of Zic3 in L-R axis development is conserved across species. Correlation of L-R patterning and C-E defects in *Xenopus* suggests early C-E defects may underlie L-R patterning defects at later stages, since Zic3 morphants with moderate to severe C-E defects exhibited an increase in laterality defects. Taken together, these results demonstrate a functional conservation of Zic3 in L-R patterning and uncover a previously unrecognized role for Zic3 in C-E morphogenesis during early vertebrate development.

Keywords

convergence extension; left-right patterning; heterotaxy; axis formation; cardiovascular malformation

INTRODUCTION

ZIC3 is a zinc finger transcription factor of the GLI superfamily. Loss of function mutations in ZIC3 result in X-linked heterotaxy, a syndrome consisting of left-right (L-R) patterning

*Corresponding author: Stephanie M. Ware, MD, PhD, Cincinnati Children's Hospital Medical Center, 240 Albert Sabin Way, MLC 7020, Cincinnati, OH 45229-3039, Phone: 513-636-9427, Fax: 513-636-5958, stephanie.ware@cchmc.org.

defects of the visceral organs, midline abnormalities and cardiac malformations (Gebbia et al., 1997; Ware et al., 2004). There are five *Zic* genes(*Zic1–5*) in human, mouse and *Xenopus laevis* (Aruga et al., 1996; Aruga et al., 1994; Brown et al., 1998; Fujimi et al., 2006; Gebbia, et al., 1997; Yokota et al., 1996). Seven *zic* genes (*zic1*, *zic2a*, *zic2b*, *zic3*, *zic4*, *zic5* and *zic6*) have been described in zebrafish (Merzdorf, 2007). Across species, Zic proteins are highly conserved within their DNA-binding domains, which consist of five C_2H_2 zinc-finger motifs (Aruga, 2004; Herman et al., 2002; Keller, et al., 2007). Despite the high conservation and close evolutionary relationship of the *Zic* gene family, only *Zic3* has been shown to be required for proper L-R asymmetry.

L-R patterning depends on a conserved pathway that includes asymmetric TGFβ signaling on the left side of the embryo (Shiratori et al., 2006; Whitman et al., 2001). Nodal, a TGFβ ligand, activates asymmetric expression of the transcription factor *Pitx2* which is thought to mediate L-R morphogenesis of developing organs. *Zic3* null mice exhibit L-R asymmetry defects recapitulating human heterotaxy syndrome (Purandare et al., 2002; Ware et al., 2006b). *Zic3* null embryos fail to maintain *Nodal* expression, and Zic3 has been shown to activate a Nodal enhancer in *Xenopus* and mouse (Ware et al., 2006a). Later in development, *Zic3* null mice exhibit randomization of *Nodal* and *Pitx2* in the lateral plate mesoderm, as well as abnormalities of asymmetric organs including the heart, lung, liver and spleen (Purandare, et al., 2002). These findings emphasize a role for Zic3 upstream of Nodal signaling in specifying L-R asymmetry.

Previous studies have also implicated Zic3 in early embryo patterning and differentiation (Lim et al., 2010; Lim et al., 2007; Ware, et al., 2006b). Loss of *Z* in *ic3* embryonic stem cells leads to loss of pluripotency and ultimately endoderm differentiation (Lim, et al., 2007). *In vivo*, *Zic3* null mice exhibit abnormalities of anterior visceral endoderm patterning (Lim, et al., 2007; Ware, et al., 2006b). Consistent with a role in early development, *Zic3* is highly expressed in neuroectoderm and mesoderm during gastrulation of mouse, chick, *Xenopus* and zebrafish embryos (Keller, et al., 2007; Kitaguchi et al., 2000; McMahon et al., 2010; Nagai et al., 1997; Nakata et al., 1997). This conserved expression pattern suggests a potential role for Zic3 during gastrulation and axial patterning.

Zic3 null mice exhibit defective gastrulation, neural tube closure and axial patterning (Purandare, et al., 2002; Ware, et al., 2006b) indicating important roles for this transcription factor during early embryogenesis. Elongation of the anterior-posterior (AP) axis and closure of the neural tube are dependent on the morphogenetic process convergent extension (C-E), which is regulated by one of the non-canonical Wnt pathways, also known as the planar cell polarity (PCP) pathway (Keller et al., 1985; Wallingford et al., 2002). This dynamic process requires a tight balance of cell adhesion and interaction in order for cells in a tissue layer to act as one. C-E morphogenesis defects have been well characterized in *Xenopus* embryos, which include blastopore closure defects during gastrulation, flexion and shortening of the A-P axis, and impaired neural tube elongation and closure (Sokol, 1996; Sumanas et al., 2001; Wallingford et al., 2001b; Wallingford, et al., 2002). Similarly, C-E defects in mouse include a specific subtype of neural tube defect, shorter and broader body axis, as well as failure of somitic tissue to converge at the midline (Garcia-Garcia et al., 2008; Lu et al., 2004; Wang et al., 2006; Yen et al., 2009). In zebrafish, C-E defects manifest as widening of the neural plate and somites, as well as a reduction in A-P axis length (Henry et al., 2000; Topczewski et al., 2001). *Zic3* null mice exhibit thickening of the primitive streak and failure of the notochord to delaminate from the foregut tissue, which suggests defective C-E since these tissues are not able to converge properly at the midline (Purandare, et al., 2002; Ware, et al., 2006b).

To gain insight into the role of Zic3 during early embryo development, a loss of function approach was taken using *Xenopus laevis* and zebrafish as model vertebrates. This study addressed 1) the role of Zic3 during C-E morphogenesis, 2) conservation of Zic3 function during L-R patterning and 3) whether C-E defects lead to L-R patterning defects. Results from this study show that Zic3 has a conserved role in *Xenopus* and zebrafish that is essential for normal gastrulation, C-E morphogenesis and L-R patterning. In addition, this study suggests that proper C-E is a prerequisite for normal L-R axis formation in vertebrates.

MATERIALS AND METHODS

Embryo collection and staging

Xenopus laevis embryos were obtained through *in vitro* fertilization. Adult females were primed with 800–1000 U of human chorionic gonadotropin (Chorulon). Testes were isolated from adult males and stored in oocyte culture medium (OCM) at 4°C. Embryos were dejellied in 2% cysteine (Sigma, pH 7.8) and cultured in 0.01× Marc's Modified Ringer (MMR). Embryo staging was determined according to the *Xenopus laevis* developmental table (Nieuwkoop et al., 1994). Wild type AB zebrafish were purchased from the Zebrafish International Resource Center (ZIRC). Zebrafish maintenance, mating, embryo culture (Westerfield, 1995) and embryo staging (Kimmel et al., 1995) were performed as previously described.

Preparation of Zic3 RNA

RNA was isolated from stage 19 *Xenopus laevis* embryos using Trizol (Invitrogen) according to the manufacturer's protocol. A full length 1.4 kb cDNA was amplified by RT-PCR, sequenced in its entirety, and subsequently subcloned into pCS2+. RNA was generated using the mMessage mMachine kit according to the manufacturer's protocol (Ambion). Human ZIC3 RNA was generated similarly using a previously described HA-ZIC3 construct as template (Ware, et al., 2004).

In vitro transcription/translation

The TnT coupled reticulocyte lysate system (Promega) was used for *in vitro* transcription and translation in the presence of ^{35}S –Met as per the manufacturer's instructions. *Xenopus zic3* and human ZIC3 with an HA epitope tag were used as templates, with or without morpholino.

Zic3 antisense morpholino oligonucleotide design

For *Xenopus laevis*, two Zic3 antisense morpholino oligonucleotides, a translational-blocking and splice site morpholino (TB MO and SS MO, respectively), were designed (Gene Tools, LLC). The TB MO sequence was 5′ ATG ACA ATG CTA TTA GAT GGA GGA C 3′, and the SS MO, designed to the exon 2-intron 2 junction, sequence was 5′ AGC ACA TGA AGG TAA GTT TTA TTG T 3′. Both Zic3 morpholinos were fluoroscein conjugated. A control antisense morpholino was also obtained from Gene Tools, LLC with the following sequence 5′ CCT CTT ACC TCA GTT ACA ATT TAT A 3′. For Zic3 knockdown in zebrafish, a Zic3 TB MO was purchased from Gene Tools, LLC with the following sequence: 5′ TAT CAA GGA GCA TAG TCA TTG GGC T 3′. All morpholinos were resuspended and stored according to manufacturer's protocol (Gene Tools, LLC).

RT-PCR analysis of Zic3 MO efficiency

In *Xenopus*, the efficiency of Zic3 knockdown by the SS MO was analyzed via RT-PCR using*zic3* full length primers: sense 5′ CTG CTC AGC TCA TTC ATG 3′, antisense 5′ GGC CTC TCT ACA TTT TGC TC 3′ and primers designed to flank exon 2: sense 5′ TCA TAT

CAG GGT GCA TAC CG 3′, antisense 5′ TCC TCA CTG TTG GCA GAA ACC A 3′. ODC (*ornithine decarboxylase*) primers were used to verify RNA quantity and quality: sense 5′ GCC ATT GTG AAG ACT CTC TCC ATT C 3′, antisense 5′ TTC GGG TGA TTC CTT GCC AC 3′ (Heasman et al., 2000).

Embryo microinjection

Xenopus microinjections were performed in 4% Ficoll in 1/3× MMR and were targeted to the dorsal marginal zone of both dorsal blastomeres of 4-cell stage embryos. *Xenopus* embryos were injected with 5.3 ng Zic3 MO. Zebrafish embryos were injected with 7.5 ng Zic3 MO at the 1–2 cell stages. *In vitro* transcribed *Zic3* mRNA was injected into zebrafish Zic3 morphants in order to rescue heart looping (125 pg) and body axis (50 pg) phenotypes.

Whole-mount in situ hybridization (WISH)

Xenopus embryos were fixed at the desired stage in MEMFA for 2 hours at room temperature. Following fixation, embryos were dehydrated in 100% EtOH and stored at −20°C. WISH was performed as previously described (Sive et al., 2000). pMyoD, pSP73-Xbra, pBSK-Cardiac Troponin, and pCS107-Pitx2 plasmids were kindly provided by the Zorn labatory and were used to generate antisense riboprobes. Zebrafish embryos were fixed at the stages indicated and processed following the procedure previously reported (Essner et al., 2005). Antisense probes for *myoD*, *dlx3*, *southpaw* (*spaw*), *cardiac myosin light chain 2* (*cmlc2*), *forkhead box a3* (*foxa3*), *no tail* (*ntl*) were generated as described (Essner, et al., 2005). Images were captured using a Zeiss MRc AxioCam digital camera mounted on a Zeiss Discovery V12 stereomicroscope. Measurements were made using AxioVision software (Zeiss).

Anatomic and morphological analysis of embryos

Xenopus embryos were anesthetized in 0.1% benzocaine (Spectrum Chemical Company) in 0.1× MMR at stage 46 to analyze heart and gut anatomy. Once anesthetized, *Xenopus* heart morphology was analyzed and scored immediately utilizing blood flow to determine the positioning of the outflow tract (Branford et al., 2000). After fixation, WISH was performed using the cardiac marker *troponin* to mark the heart. The anatomic characterization of laterality included positioning of the heart and outflow tract, gall bladder, gut origin, and gut coiling direction (Branford, et al., 2000; Levin et al., 1998). In zebrafish embryos, heart looping was scored either in live embryos or in fixed embryos analyzed via WISH for *cmlc2* staining of the heart. Gut morphology was analyzed using WISH of *foxa3*.

RESULTS

Targeted knockdown of Zic3 results in axial patterning defects in Xenopus

To examine the role of Zic3 in early embryonic patterning, translational-blocking (TB MO) and splice site blocking (SS MO) morpholinos were designed to knockdown expression in *Xenopus* (Fig. 1A). RT-PCR and subsequent sequencing revealed that Zic3 SS MO altered splicing such that exon 2 is skipped, resulting in a frameshift and premature truncation of the Zic3 protein prior to the DNA binding domains (Fig. 1B). To test the function of the Zic3 TB MO, *in vitro* transcription-translation of a *Xenopus zic3* or human HA-ZIC3 expression plasmid was performed with ^{35}S-Met in the presence or absence of TB MO. TB MO specifically inhibited translation of *Xenopus zic3* (*Xzic3*) but not human HA-ZIC3 (Fig. 1C).

The Zic3 MOs were independently injected into the marginal zone of both dorsal blastomeres of 4-cell stage embryos to knockdown Zic3 in the dorsal mesoderm where it is highly expressed during gastrulation (Kitaguchi, et al., 2000; Nakata, et al., 1997). Zic3 morphants exhibited a variety of axial defects. A scaling system was utilized to assess the

phenotypes resulting from a single Zic3 MO dose. The scale ranged from a score of 1, indicating normal axis elongation and closure of the neural tube, to a score of 5, indicating severe dorsal flexion with neural tube defects (Fig. 1D). Both Zic3 MOs induced comparable axial defects with average scores of 2.78 (TB MO) and 2.87 (SS MO), as compared to an average score of 1.18 in control (CTRL MO) injected embryos (Fig. 1E). The consistency in phenotypes from both Zic3 MOs suggests specificity of knockdown. The Zic3 SS MO was used for additional analyses except where indicated.

Convergent extension defects in Xenopus Zic3 morphants

Defects in C-E are characterized by gastrulation defects, impaired neural tube closure, and failure to extend the A-P axis. Zic3 morphants were analyzed during gastrulation and neurulation to assess the role of Zic3 in C-E. At gastrula stage, approximately 50% of the Zic3 morphants showed delayed blastopore closure, occasionally coupled with irregular shape as assessed at stage 12 (Fig. 2B and C). Some of these embryos eventually closed their blastopores while others failed to do so resulting in an open neural tube, indicative of incomplete gastrulation. Blastopore size was measured to quantify closure at late gastrula stage using *brachyury* WISH to mark the mesoderm surrounding the blastopore (Fig. 2D and E; within white dotted line). Blastopore area measurements confirmed that Zic3 morphant embryos had blastopore closure defects compared to control MO-injected embryos (Fig. 2F). *Brachyury* expression was not perturbed in the Zic3 morphants.

At late gastrula stage, *brachyury* also marks the developing notochord, a structure that is characterized by compaction and elongation. If C-E is disrupted, the notochord fails to elongate, resulting in a lower length to width ratio (Wallingford et al., 2001a). Analysis of the notochord in injected embryos revealed that the average length to width ratio was significantly reduced in Zic3 morphants relative to CTRL MO-injected embryos (Fig. 2G–I).

To assess extension of the A-P axis, embryos were measured from cement gland to tail tip (Fig. 2J and K). Zic3 morphants had a shorter average A-P axis length than CTRL MO embryos (Fig. 2K and 2 L). This finding is consistent with the average C-E phenotype score ~3 seen in the Zic3 morphants (Fig. 1E). Taken together, the results demonstrate that *Xenopus* Zic3 morphants exhibit blastopore closure, notochord elongation and A-P axis defects that are consistent with a disruption of C-E morphogenesis.

The requirement for Zic3 in axis formation is conserved across species

To test whether the role of Zic3 during early development is conserved across species a MO was designed to knockdown *zic3* expression in zebrafish. Similar to *Xenopus* Zic3 morphants, zebrafish Zic3 morphants developed phenotypes associated with C-E defects. During gastrulation, WISH analysis of *no tail*, a zebrafish ortholog of *brachyury*, showed that the developing notochord tissue was wide and loosely packed in the majority of Zic3 morphants instead of tightly condensed as seen in the stage-matched controls (Fig. 3A–D). At early somite stages, WISH markers revealed an increased width of somites (white line in Fig. 3E, F) and the neural plate (red line in Fig. 3E, F) in Zic3 morphants as compared to controls. Increased somite and neural plate widths are indicative of a failure of cells to converge towards the midline. To quantify this effect, we measured the width of the anterior neural plate (red line in Fig. 3E, F), which was wider in Zic3 morphants than in controls (Fig. 3G). In addition, Zic3 morphants showed defects in A/P axis elongation, as indicated by an increased distance between the head and tail (Fig. 3H–J). At 2 days post-fertilization (dpf), Zic3 morphants exhibited severe curvature and shortening of the A/P body axis with 76% of morphants demonstrating a short body axis as compared to 6% of control embryos (Fig. 3K, show representative L images; Fig. 4E shows quantitative results). At 5 dpf, A/P axis defects persisted in Zic3 morphants and these embryos often developed edema (Fig.

4C). Importantly, co-injection of Zic3 MO with *Xenopus zic3* mRNA, which alone had little effect on axial patterning (Fig. 4B, E), was able to rescue the axial defects caused by Zic3 MO (Fig. 4C–E). These results indicate axial phenotypes observed in Zic3 morphants are due specifically to loss of Zic3 function, and that Zic3 plays a conserved role in axis formation.

Zic3 has a conserved role in specifying left-right asymmetry

During normal vertebrate development, the heart and gut become asymmetric along the L-R axis. Loss of Zic3 function in humans and mice disrupts organ L-R asymmetry (Gebbia, et al., 1997; Purandare, et al., 2002; Ware, et al., 2006b; Ware, et al., 2004). In *Xenopus*, the cardiac outflow tract stems from the right side of the heart and loops towards the left side (Fig. 5A). *Xenopus* Zic3 morphants exhibited an increase in heart looping abnormalities compared to control embryos (Fig. 5D; Zic3 MO 34%, n= 127; CTRL MO 12%, n= 133). These gross abnormalities included a mirror reversal dextrocardia phenotype and an ambiguous phenotype, characterized by a wide variety of looping or morphologic abnormalities of the outflow tract or heart (Figs. 5B and 5 C). Laterality defects of the gut were also observed in Zic3 morphants. The developing *Xenopus* gut originates on the embryo's right side (right origin, RO), and coils in a counter-clockwise (CCW) direction (Fig. 5E). Mirror image reversal (left origin, LO, and clockwise coiling direction, CW) was identified in 7% of Zic3 morphants compared to 4% in control morphants (Fig. 5F, J). Gut anatomy categorized as abnormal included embryos with other combinations of abnormal origin or coiling (Fig. 5G, H) and ambiguous embryos (Fig. 5I; Zic3 MO 44%, n= 127; CTRL MO 6%, n=133). Abnormal gut coiling, also known as malrotation, is a frequently identified feature of human heterotaxy (Lin et al., 2000).

Zic3 knockdown in zebrafish also resulted in heart and gut laterality defects. In contrast to normal rightward looping of the heart observed in controls, the heart often failed to loop or showed a mirror reversal in Zic3 morphants (Fig. 6D; Zic3 MO 48%, n=81; Control 7%, n=58). *Xenopus zic3* mRNA was able to rescue these heart laterality defects (Fig. 6D), indicating this effect is specific to loss of Zic3 function. In addition, these results demonstrate that, similar to convergent extension defects, Xenopuszic3 mRNA is able to rescue L-R patterning abnormalities.

Zebrafish Zic3 morphants also showed gut laterality and patterning defects (Fig. 6F–H). The most common defect was a mirror reversal of the placement of the liver and pancreas. Ambiguous patterning of liver and pancreas, including multiple embryos with accessory structures, was common. Together, these results demonstrate a conserved role for Zic3 in establishing normal organ laterality.

Laterality of organs is controlled by asymmetric expression of a conserved Nodal-Pitx2 signaling cascade. To determine whether Zic3 functions upstream of Nodal-Pitx2 asymmetry, WISH was used to analyze expression of *pitx2* in *Xenopus* and the Nodal-related gene *southpaw* (*spaw*) in zebrafish, both of which are normally expressed in left lateral plate mesoderm. Abnormal *pitx2* and *spaw* expression patterns were identified in a majority of *Xenopus* and zebrafish Zic3 morphants, confirming the function of Zic3 upstream of Nodal signal transduction (Fig. 7).

Correlation between convergent extension and left-right asymmetry

To understand the potential effect of defective C-E morphogenesis on L-R patterning, a subset of control MO and Zic3 SS MO-injected *Xenopus* embryos were further analyzed based on their C-E phenotype score and their *pitx2* expression pattern. As described, Zic3 morphants exhibited a higher incidence of C-E defects (Fig. 8A) and L-R defects (Fig. 8B)

than control MO-injected embryos. Analysis of defective C-E morphogenesis and L-R patterning, using *pitx2* expression, in the same embryos revealed that disruption of C-E correlated with increased L-R patterning abnormalities (Fig. 8C). Interestingly, *pitx2* expression was also abnormal in nearly 90% of the small subset of control MO-injected embryos with severe C-E defects. This result suggests that the correlation of L-R patterning abnormalities with severity of C-E defects is generalizable (Fig. 8C). In addition, Zic3 morphants with severe C-E phenotypes exhibited an increase in L-R patterning defects compared to Zic3 morphants with normal to mild C-E phenotypes (Fig. 8C). Taken together, these results suggest that Zic3 is necessary for both L-R patterning and C-E morphogenesis, and that aberrant C-E morphogenesis exacerbates L-R patterning defects.

DISCUSSION

The proper formation and patterning of the left and right body axes are critically important processes during embryonic development, with disturbances resulting in a variety of congenital anomalies, the most classic of which is heterotaxy syndrome. Animal models have been invaluable for identifying a canonical TGFβ signaling pathway that is required for proper L-R patterning and is conserved across species. However, there remain fundamental questions about genetic pathways operating upstream and downstream of this conserved TGFβ pathway, such as whether they are species-specific or conserved, whether they are relevant for human disease, and how they are mechanistically integrated with Nodal signal transduction. In this context, it is important to understand the function of Zic3, the first gene unequivocally shown to cause human heterotaxy. This study is the first phenotypic analysis of Zic3 using a loss of function approach in *Xenopus* and zebrafish via morpholino antisense oligonucleotides. The results of this study establish a highly conserved role for Zic3 in gastrulation and L-R patterning of *Xenopus laevis* and zebrafish, providing important insight into the function of this transcription factor during development.

Zic3 morphants and gastrulation defects

The *Zic3* knock out mouse model demonstrated embryonic patterning defects during early gastrulation, a phenotype not anticipated by studying pedigrees of families with ZIC3 mutations. Because of the difficulties of analysis in mouse, we sought to develop other model organisms to better understand the function of Zic3 during early development. The gastrulation and laterality defects in *Xenopus* and zebrafish Zic3 morphants recapitulate the phenotypes observed in *Zic3* null mice and human heterotaxy syndrome, indicating that *Xenopus* and zebrafish are reliable and higher throughput models to study these early processes. Previous data have placed Zic3 downstream of Brachyury during gastrulation by virtue of the fact that an inducible form of *brachyury* (*Xbra*) rapidly induces *zic3* expression (Kitaguchi et al., 2002). Data herein demonstrate that Zic3 does not regulate *brachyury* expression, indicating a lack of a regulatory loop. However, Zic3 morphants demonstrate abnormalities in tissues that require C-E for proper formation in both *Xenopus* and zebrafish, providing novel insight into the developmental role of Zic3.

Determining whether the range of anomalies identified in Zic3 mutants are a result of distinct stage- and tissue-specific roles of this transcription factor or a downstream effect of early gastrulation abnormalities is an important question for future research. While there is some evidence to suggest that C-E defects and L-R patterning defects are linked events, as discussed below, determination of the developmental stage-specific requirement for Zic3 during gastrulation and later organogenesis will require temporal or conditional loss of function approaches to test directly.

While Zic3 appears to have a unique role during L-R patterning amongst the *Zic* family genes, other family members are expressed in similar patterns during gastrulation and their

functions have not been well studied at these stages. This work suggests that further investigation of the function of Zic family members during early embryonic stages may be important for understanding early morphogenetic events. Redundant or compensatory functions of the family members during gastrulation are potential explanations for the phenotypic variability identified in Zic3 morphants and *Zic3* null mice. One previous study has shown that *Zic1* expression is increased when Zic3 is knocked down in *Xenopus*, suggesting reciprocal regulation (Marchal et al., 2009). Likewise, during organogenesis there is evidence for overlapping functions of Zic gene family members. For example, *Zic2* and *Zic3* have been shown to have synergistic effects on axial patterning and neurulation (Inoue et al., 2007). Analysis of altered expression of other *Zic* genes will be valuable in determining whether other *Zic* genes may compensate for loss of *Zic3* function.

Zic3 and L-R patterning

Human heterotaxy is a genetically and clinically heterogeneous multiple congenital anomaly syndrome. ZIC3 mutations were initially shown to cause heterotaxy in families demonstrating X-linked inheritance (Gebbia, et al., 1997). Subsequently, ZIC3 mutations were also identified in patients with isolated congenital heart disease and in patients previously thought to have other syndromic associations such as VACTERL (Chung et al., 2011; Megarbane et al., 2000; Ware, et al., 2004; Wessels et al., 2010). *In vitro* and *in vivo* analyses confirm that L-R patterning abnormalities result from of loss of function of Zic3 (Bedard et al., 2007; Purandare, et al., 2002; Ware, et al., 2004). Because Zic3 is highly conserved across species, we investigated whether its function in L-R patterning is similarly conserved. The morphant analyses presented here demonstrate that Zic3 is critical for L-R patterning in zebrafish and *Xenopus*, in addition to its previously described roles in mouse and human. Zic3 is highly conserved at the nucleotide and amino acid level across species. The morphant analyses in the current study indicate that *Xenopus* Zic3 can rescue knock-down of zebrafish Zic3 loss of function, indicating an important functional conservation.

In mouse, current models suggest that L-R asymmetry initiates at the node and is dependent on the function of motile cilia and leftward fluid flow. However, in chick, *Xenopus*, and zebrafish, there is evidence for L-R asymmetry at earlier developmental stages. In chick, motile cilia have not been identified. Rather, cellular movements around Hensen's node are required for later asymmetric expression of molecular markers at the organizer (Cui et al., 2009; Gros et al., 2009). In *Xenopus*, intracellular asymmetries are apparent at the one cell stage and models that focus on cytoskeletal transport, electrochemical gradients, and chromatid segregation have been proposed to explain the early generation of intracellular L-R asymmetry (reviewed in (Vandenberg et al., 2010). It remains to be determined how these early laterality mechanisms are later integrated with cilia function to determine organ laterality. The fact that Zic3 function in gastrulation and L-R patterning is conserved across species therefore represents an important opportunity to unify disparate models of asymmetry in these organisms and further evaluate the paradigm of L-R initiating at the node in mouse.

The relationship of L-R asymmetry and C-E morphogenesis

This study also addresses the relationship of C-E morphogenesis and L-R patterning, which has not been carefully examined in many studies focusing on L-R defects. We find a correlation between C-E defects and L-R defects in Zic3 morphants (Fig. 8). Zic3 morphants with C-E defects that survived for later stage analysis demonstrated bilateral or absent expression of L-R molecular markers indicating a failure to establish laterality. Furthermore, the finding of L-R defects in the small subset of control embryos that had severe C-E defects argues that proper C-E is a prerequisite for the development of normal laterality. This finding is in agreement with recent studies that linked defective PCP of the cells that

comprise the mouse node and *Xenopus* gastrocoel roof plate (GRP) with random positioning of the motile cilia within the organizer, which ultimately results in aberrant L-R patterning (Antic et al., 2010; Song et al., 2010). Core PCP proteins may be necessary but not sufficient for basal body polarization and ciliogenesis at the node (Jones et al., 2008). For example, defects have been identified in mutants such as *fuzzy* and *inturned* in which Shh signaling participates with PCP core proteins for ciliogenesis (Park et al., 2006). Given that Zic3 is known to physically and functionally interact with Gli proteins that mediate Shh signaling, future work to determine its developmental interactions with effectors of PCP and ciliogenesis is necessary.

CONCLUSIONS

This study is the first to show that Zic3 has a conserved role in *Xenopus* and zebrafish for L-R patterning, gastrulation, and C-E morphogenesis. In addition, this study demonstrates that proper C-E is a prerequisite for normal L-R axis formation, and suggests that this mechanism is broadly conserved across species.

Supplementary Material

Refer to Web version on PubMed Central for supplementary material.

Acknowledgments

We thank the Heasman and Zorn labs at CCHMC for reagents and technical expertise and F. Foley at SUNY Upstate for technical assistance. This work was supported by funding from a CCHMC trustees grant (S.M.W.), NIH HL088639 (S.M.W.) and March of Dimes Basil O'Connor Starter Scholar award (J.D.A.).

References

Antic D, Stubbs JL, Suyama K, Kintner C, Scott MP, Axelrod JD. Planar cell polarity enables posterior localization of nodal cilia and left-right axis determination during mouse and Xenopus embryogenesis. PLoS One. 2010; 5:e8999. [PubMed: 20126399]

Aruga J. The role of Zic genes in neural development. Mol Cell Neurosci. 2004; 26:205–221. [PubMed: 15207846]

Aruga J, Nagai T, Tokuyama T, Hayashizaki Y, Okazaki Y, Chapman VM, Mikoshiba K. The mouse zic gene family. Homologues of the Drosophila pair-rule gene odd-paired. J Biol Chem. 1996; 271:1043–1047. [PubMed: 8557628]

Aruga J, Yokota N, Hashimoto M, Furuichi T, Fukuda M, Mikoshiba K. A novel zinc finger protein, zic, is involved in neurogenesis, especially in the cell lineage of cerebellar granule cells. J Neurochem. 1994; 63:1880–1890. [PubMed: 7931345]

Bedard JE, Purnell JD, Ware SM. Nuclear import and export signals are essential for proper cellular trafficking and function of ZIC3. Hum Mol Genet. 2007; 16:187–198. [PubMed: 17185387]

Branford WW, Essner JJ, Yost HJ. Regulation of gut and heart left-right asymmetry by context-dependent interactions between xenopus lefty and BMP4 signaling. Dev Biol. 2000; 223:291–306. [PubMed: 10882517]

Brown SA, Warburton D, Brown LY, Yu CY, Roeder ER, Stengel-Rutkowski S, Hennekam RC, Muenke M. Holoprosencephaly due to mutations in ZIC2, a homologue of Drosophila odd-paired. Nat Genet. 1998; 20:180–183. [PubMed: 9771712]

Chung B, Shaffer LG, Keating S, Johnson J, Casey B, Chitayat D. From VACTERL-H to heterotaxy: variable expressivity of ZIC3-related disorders. Am J Med Genet A. 2011; 155A:1123–1128. [PubMed: 21465648]

Cui C, Little CD, Rongish BJ. Rotation of organizer tissue contributes to left-right asymmetry. Anat Rec (Hoboken). 2009; 292:557–561. [PubMed: 19301278]

Essner JJ, Amack JD, Nyholm MK, Harris EB, Yost HJ. Kupffer's vesicle is a ciliated organ of asymmetry in the zebrafish embryo that initiates left-right development of the brain, heart and gut. Development. 2005; 132:1247–1260. [PubMed: 15716348]

Fujimi TJ, Mikoshiba K, Aruga J. Xenopus Zic4: conservation and diversification of expression profiles and protein function among the Xenopus Zic family. Dev Dyn. 2006; 235:3379–3386. [PubMed: 16871625]

Garcia-Garcia MJ, Shibata M, Anderson KV. Chato, a KRAB zinc-finger protein, regulates convergent extension in the mouse embryo. Development. 2008; 135:3053–3062. [PubMed: 18701545]

Gebbia M, Ferrero GB, Pilia G, Bassi MT, Aylsworth A, Penman-Splitt M, Bird LM, Bamforth JS, Burn J, Schlessinger D, Nelson DL, Casey B. X-linked situs abnormalities result from mutations in ZIC3. Nat Genet. 1997; 17:305–308. [PubMed: 9354794]

Gros J, Feistel K, Viebahn C, Blum M, Tabin CJ. Cell movements at Hensen's node establish left/right asymmetric gene expression in the chick. Science. 2009; 324:941–944. [PubMed: 19359542]

Heasman J, Kofron M, Wylie C. Beta-catenin signaling activity dissected in the early Xenopus embryo: a novel antisense approach. Dev Biol. 2000; 222:124–134. [PubMed: 10885751]

Henry CA, Hall LA, Burr Hille M, Solnica-Krezel L, Cooper MS. Somites in zebrafish doubly mutant for knypek and trilobite form without internal mesenchymal cells or compaction. Curr Biol. 2000; 10:1063–1066. [PubMed: 10996075]

Herman GE, El-Hodiri HM. The role of ZIC3 in vertebrate development. Cytogenet Genome Res. 2002; 99:229–235. [PubMed: 12900569]

Inoue T, Ota M, Mikoshiba K, Aruga J. Zic2 and Zic3 synergistically control neurulation and segmentation of paraxial mesoderm in mouse embryo. Dev Biol. 2007; 306:669–684. [PubMed: 17490632]

Jones C, Roper VC, Foucher I, Qian D, Banizs B, Petit C, Yoder BK, Chen P. Ciliary proteins link basal body polarization to planar cell polarity regulation. Nat Genet. 2008; 40:69–77. [PubMed: 18066062]

Keller MJ, Chitnis AB. Insights into the evolutionary history of the vertebrate zic3 locus from a teleost-specific zic6 gene in the zebrafish, Danio rerio. Dev Genes Evol. 2007; 217:541–547. [PubMed: 17503076]

Keller RE, Danilchik M, Gimlich R, Shih J. The function and mechanism of convergent extension during gastrulation of Xenopus laevis. J Embryol Exp Morphol. 1985; 89(Suppl):185–209. [PubMed: 3831213]

Kimmel CB, Ballard WW, Kimmel SR, Ullmann B, Schilling TF. Stages of embryonic development of the zebrafish. Dev Dyn. 1995; 203:253–310. [PubMed: 8589427]

Kitaguchi T, Mizugishi K, Hatayama M, Aruga J, Mikoshiba K. Xenopus Brachyury regulates mesodermal expression of Zic3, a gene controlling left-right asymmetry. Dev Growth Differ. 2002; 44:55–61. [PubMed: 11869292]

Kitaguchi T, Nagai T, Nakata K, Aruga J, Mikoshiba K. Zic3 is involved in the left-right specification of the Xenopus embryo. Development. 2000; 127:4787–4795. [PubMed: 11044394]

Levin M, Mercola M. Gap junctions are involved in the early generation of left-right asymmetry. Dev Biol. 1998; 203:90–105. [PubMed: 9806775]

Lim LS, Hong FH, Kunarso G, Stanton LW. The pluripotency regulator Zic3 is a direct activator of the Nanog promoter in ESCs. Stem Cells. 2010; 28:1961–1969. [PubMed: 20872845]

Lim LS, Loh YH, Zhang W, Li Y, Chen X, Wang Y, Bakre M, Ng HH, Stanton LW. Zic3 is required for maintenance of pluripotency in embryonic stem cells. Mol Biol Cell. 2007; 18:1348–1358. [PubMed: 17267691]

Lin AE, Ticho BS, Houde K, Westgate MN, Holmes LB. Heterotaxy: associated conditions and hospital-based prevalence in newborns. Genet Med. 2000; 2:157–172. [PubMed: 11256661]

Lu X, Borchers AG, Jolicoeur C, Rayburn H, Baker JC, Tessier-Lavigne M. PTK7/CCK-4 is a novel regulator of planar cell polarity in vertebrates. Nature. 2004; 430:93–98. [PubMed: 15229603]

Marchal L, Luxardi G, Thome V, Kodjabachian L. BMP inhibition initiates neural induction via FGF signaling and Zic genes. Proc Natl Acad Sci U S A. 2009; 106:17437–17442. [PubMed: 19805078]

McMahon AR, Merzdorf CS. Expression of the zic1, zic2, zic3, and zic4 genes in early chick embryos. BMC Res Notes. 2010; 3:167. [PubMed: 20553611]

Megarbane A, Salem N, Stephan E, Ashoush R, Lenoir D, Delague V, Kassab R, Loiselet J, Bouvagnet P. X-linked transposition of the great arteries and incomplete penetrance among males with a nonsense mutation in ZIC3. Eur J Hum Genet. 2000; 8:704–708. [PubMed: 10980576]

Merzdorf CS. Emerging roles for zic genes in early development. Dev Dyn. 2007; 236:922–940. [PubMed: 17330889]

Nagai T, Aruga J, Takada S, Gunther T, Sporle R, Schughart K, Mikoshiba K. The expression of the mouse Zic1, Zic2, and Zic3 gene suggests an essential role for Zic genes in body pattern formation. Dev Biol. 1997; 182:299–313. [PubMed: 9070329]

Nakata K, Nagai T, Aruga J, Mikoshiba K. Xenopus Zic3, a primary regulator both in neural and neural crest development. Proc Natl Acad Sci U S A. 1997; 94:11980–11985. [PubMed: 9342348]

Park TJ, Haigo SL, Wallingford JB. Ciliogenesis defects in embryos lacking inturned or fuzzy function are associated with failure of planar cell polarity and Hedgehog signaling. Nat Genet. 2006; 38:303–311. [PubMed: 16493421]

Purandare SM, Ware SM, Kwan KM, Gebbia M, Bassi MT, Deng JM, Vogel H, Behringer RR, Belmont JW, Casey B. A complex syndrome of left-right axis, central nervous system and axial skeleton defects in Zic3 mutant mice. Development. 2002; 129:2293–2302. [PubMed: 11959836]

Shiratori H, Hamada H. The left-right axis in the mouse: from origin to morphology. Development. 2006; 133:2095–2104. [PubMed: 16672339]

Sokol SY. Analysis of Dishevelled signalling pathways during Xenopus development. Curr Biol. 1996; 6:1456–1467. [PubMed: 8939601]

Song H, Hu J, Chen W, Elliott G, Andre P, Gao B, Yang Y. Planar cell polarity breaks bilateral symmetry by controlling ciliary positioning. Nature. 2010; 466:378–382. [PubMed: 20562861]

Sumanas S, Ekker SC. Xenopus frizzled-7 morphant displays defects in dorsoventral patterning and convergent extension movements during gastrulation. Genesis. 2001; 30:119–122. [PubMed: 11477687]

Topczewski J, Sepich DS, Myers DC, Walker C, Amores A, Lele Z, Hammerschmidt M, Postlethwait J, Solnica-Krezel L. The zebrafish glypican knypek controls cell polarity during gastrulation movements of convergent extension. Dev Cell. 2001; 1:251–264. [PubMed: 11702784]

Vandenberg LN, Levin M. Far from solved: a perspective on what we know about early mechanisms of left-right asymmetry. Dev Dyn. 2010; 239:3131–3146. [PubMed: 21031419]

Wallingford JB, Ewald AJ, Harland RM, Fraser SE. Calcium signaling during convergent extension in Xenopus. Curr Biol. 2001a; 11:652–661. [PubMed: 11369228]

Wallingford JB, Harland RM. Xenopus Dishevelled signaling regulates both neural and mesodermal convergent extension: parallel forces elongating the body axis. Development. 2001b; 128:2581–2592. [PubMed: 11493574]

Wallingford JB, Harland RM. Neural tube closure requires Dishevelled-dependent convergent extension of the midline. Development. 2002; 129:5815–5825. [PubMed: 12421719]

Wang J, Hamblet NS, Mark S, Dickinson ME, Brinkman BC, Segil N, Fraser SE, Chen P, Wallingford JB, Wynshaw-Boris A. Dishevelled genes mediate a conserved mammalian PCP pathway to regulate convergent extension during neurulation. Development. 2006; 133:1767–1778. [PubMed: 16571627]

Ware SM, Harutyunyan KG, Belmont JW. Heart defects in X-linked heterotaxy: evidence for a genetic interaction of Zic3 with the nodal signaling pathway. Dev Dyn. 2006a; 235:1631–1637. [PubMed: 16496285]

Ware SM, Harutyunyan KG, Belmont JW. Zic3 is critical for early embryonic patterning during gastrulation. Dev Dyn. 2006b; 235:776–785. [PubMed: 16397896]

Ware SM, Peng J, Zhu L, Fernbach S, Colicos S, Casey B, Towbin J, Belmont JW. Identification and functional analysis of ZIC3 mutations in heterotaxy and related congenital heart defects. Am J Hum Genet. 2004; 74:93–105. [PubMed: 14681828]

Wessels MW, Kuchinka B, Heydanus R, Smit BJ, Dooijes D, de Krijger RR, Lequin MH, de Jong EM, Husen M, Willems PJ, Casey B. Polyalanine expansion in the ZIC3 gene leading to X-linked

heterotaxy with VACTERL association: a new polyalanine disorder? J Med Genet. 2010; 47:351–355. [PubMed: 20452998]

Whitman M, Mercola M. TGF-beta superfamily signaling and left-right asymmetry. Sci STKE. 2001; 2001:re1. [PubMed: 11752633]

Yen WW, Williams M, Periasamy A, Conaway M, Burdsal C, Keller R, Lu X, Sutherland A. PTK7 is essential for polarized cell motility and convergent extension during mouse gastrulation. Development. 2009; 136:2039–2048. [PubMed: 19439496]

Yokota N, Aruga J, Takai S, Yamada K, Hamazaki M, Iwase T, Sugimura H, Mikoshiba K. Predominant expression of human zic in cerebellar granule cell lineage and medulloblastoma. Cancer Res. 1996; 56:377–383. [PubMed: 8542595]

Highlights

- Zebrafish and Xenopus can be used to study human X-linked heterotaxy
- We identify a novel role for Zic3 in convergent-extension morphogenesis
- Early convergent-extension defects may underlie laterality defects at later stages

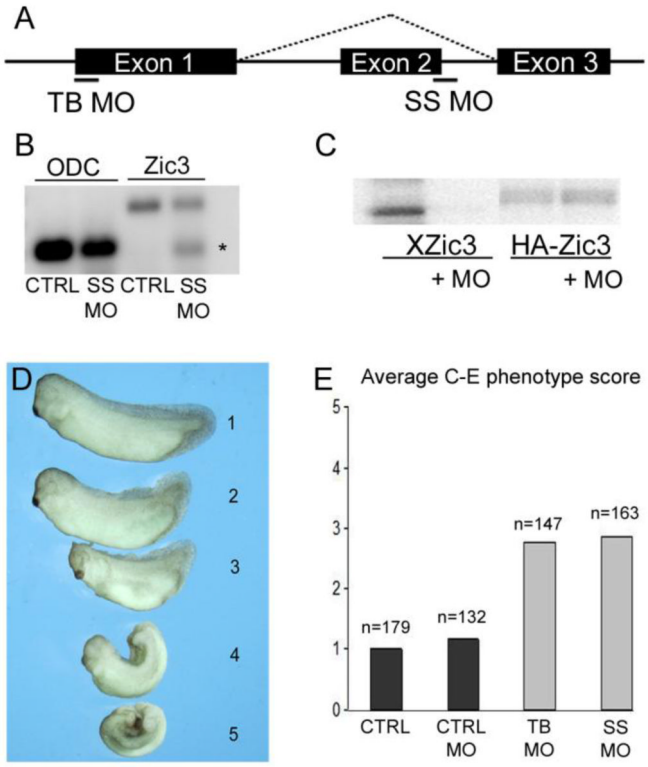

Fig. 1.

Knockdown of Zic3 disrupts axial development in *Xenopus*. (A) Schematic of *zic3* exon-intron structure showing translational-blocking (TB) and splice site blocking (SS) morpholino target sites. (B) RT-PCR analysis of *zic3* in control (CTRL) and SS MO injected embryos. Asterisk denotes product that lacks exon 2. The top band is the full-length *zic3* product. ODC was used as a loading control. (C) *In vitro* transcription-translation using *Xenopus zic3* (*Xzic3*) or human HA-*ZIC3* expression plasmids in the presence or absence of Zic3 TB MO.

(D) Scaling system used to score *Xenopus* Zic3 morphant phenotypes that ranged from normal (1) to severe dorsal flexion with neural tube defect (5). (E) Average scores of control (CTRL), control morpholino (CTRL MO), Zic3 translational-blocking MO (TB MO), and Zic3 splice site morpholino (SS MO) injected embryos. Number of embryos (n) scored is shown above each injection group.

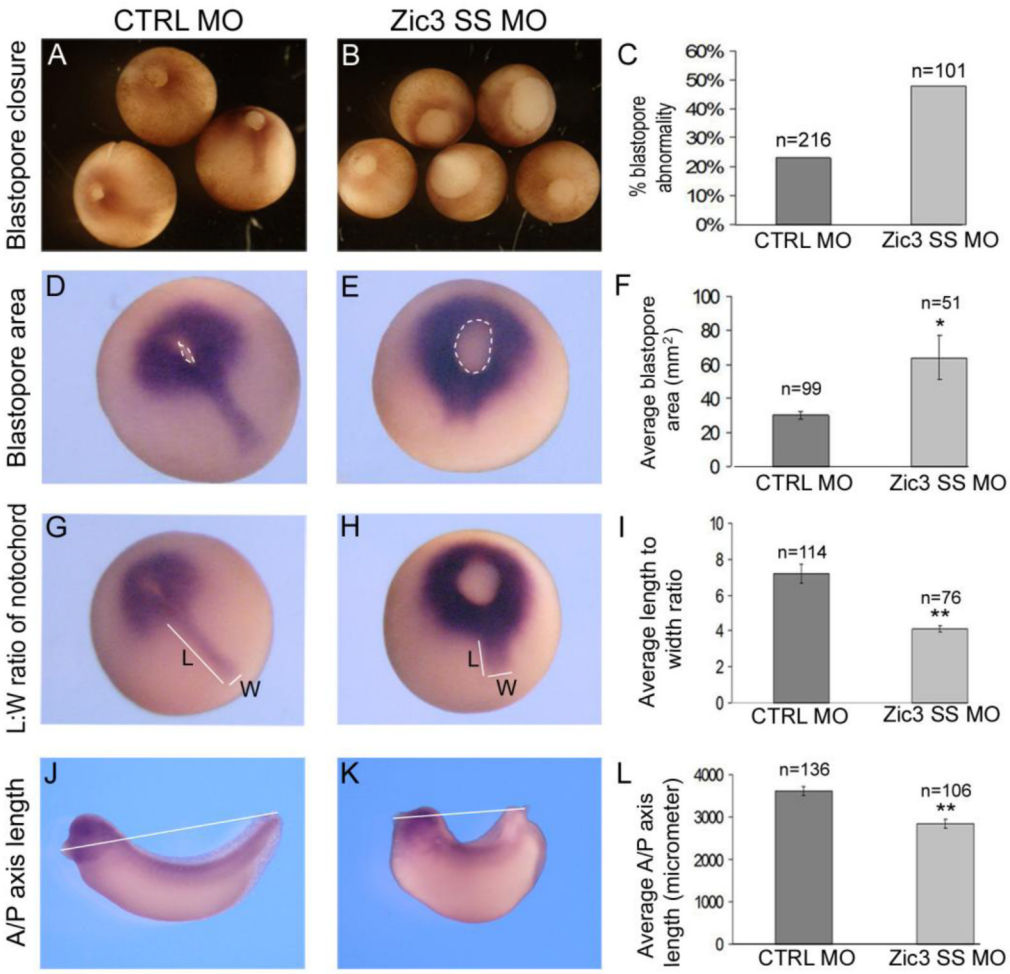

Fig. 2.

Xenopus Zic3 morphants exhibit defective gastrulation and convergent extension morphogenesis. (A) Normal control (CTRL) MO embryos at gastrula stage. (B) Sibling Zic3 morphants at stage 12.25 with delayed and abnormal blastopore closure. (C) The percentage of control morpholino and Zic3 morphant embryos that showed blastopore closure defects. (D–E, G–H) Whole-mount *in situ* hybridization (WISH) of *brachyury* at stage 13. (D) The blastopore area is outlined by the dashed line in control morpholino (D) and Zic3 morphant (E) embryos. (F) Average blastopore area in control and Zic3 morphant embryos. (G) Notochord length (L) and width (W) are designated by white lines in control morpholino embryos (G) and Zic3 morphants (H), which exhibited a wider, shorter notochord. (I) Average notochord length-to-width ratio in control morpholino and Zic3 morphant embryos. (J) Anterior-posterior (A-P) axis measurement (white line) of control morphant (J) and Zic3 morphant (K) embryos at the tailbud stage. (L) Average A-P axis lengths in control and Zic3 morphants. Error bars represent SEM. *$p<0.05$; **$p<0.01$ by *t*-test.

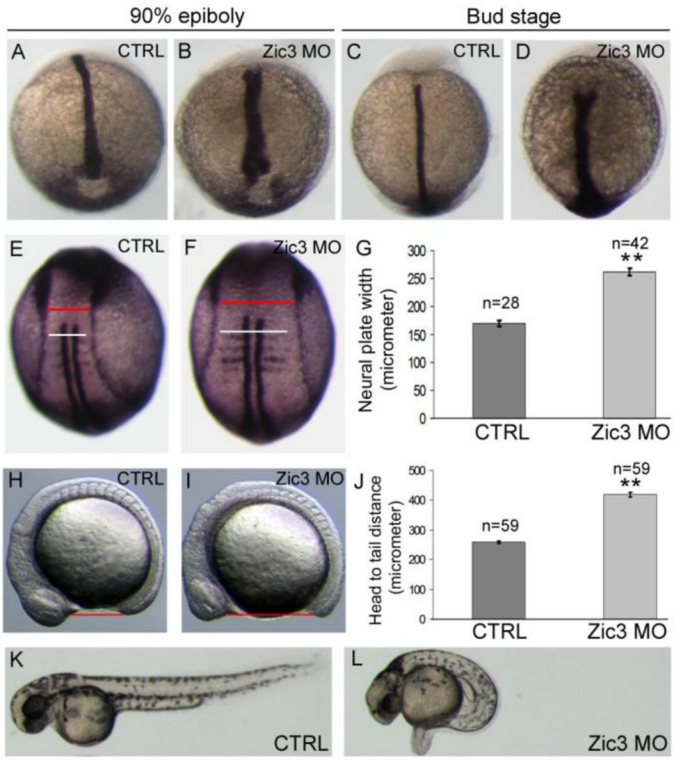

Fig. 3.

Convergent extension and axial defects in Zic3 morphant zebrafish. (A–D) WISH of *no tail* expression in the notochord at 90% epiboly (A,B) and tailbud (C,D) stages. Control (CTRL) embyos (A,C) showed normal notochord development, whereas Zic3 morphants (B,D) exhibited a broader notochord. (E,F) WISH of *myod* and *dlx3b* at the 4-somite stage to label somites and the neural plate border, respectively. The red lines mark the width of the neural plate and the white lines indicate somite width. (G) Average width of the neural plate (measured at the red line) in control and Zic3 morphant embryos. (H,I) Live control (H) and Zic3 morphant (I) embryos at the 12-somite stage. The red lines indicate head-to-tail distance. (J) Average head-to-tail distances in control and Zic3 morphants. Live control (K) and Zic3 morphant (L) embryos at 2 days post-fertilization. Error bars represent SEM. $^{**}p<0.01$ by *t*-test.

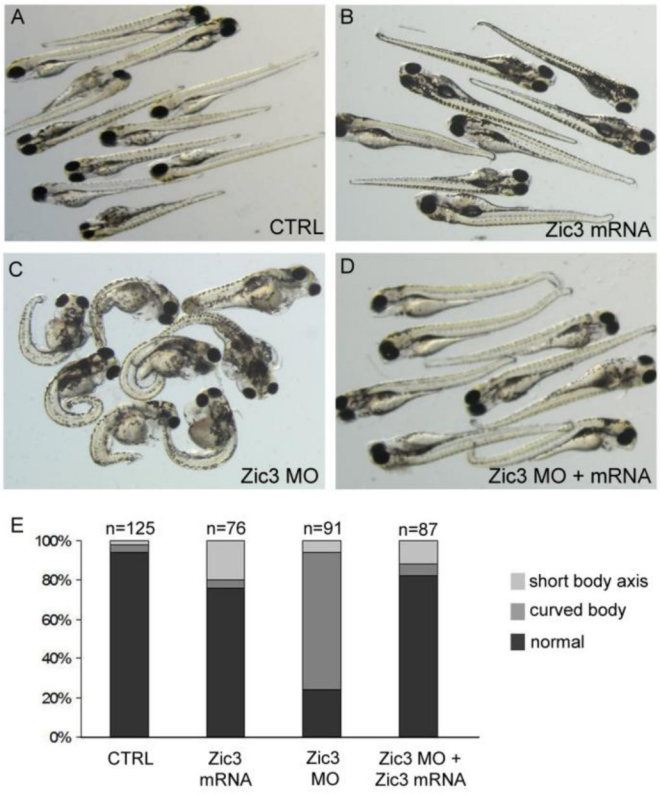

Fig. 4.

Xenopus zic3 rescues axial defects in zebrafish Zic3 morphants. (A–D) Live embryos at 5 days post-fertilization. (A) Uninjected control embryos. (B) *Xzic3* mRNA-injected embryos showed subtle phenotypes including a curled tail tip. (C) Zic3 morphant embryos had a shortened and curved A-P axis and edema. (D) Embryos co-injected with Zic3 morpholino and *Xzic3* mRNA. (E) Percentage of embryos with a curved or shortened axis. Embryos with minor curled tail tips were scored to have normal body elongation.

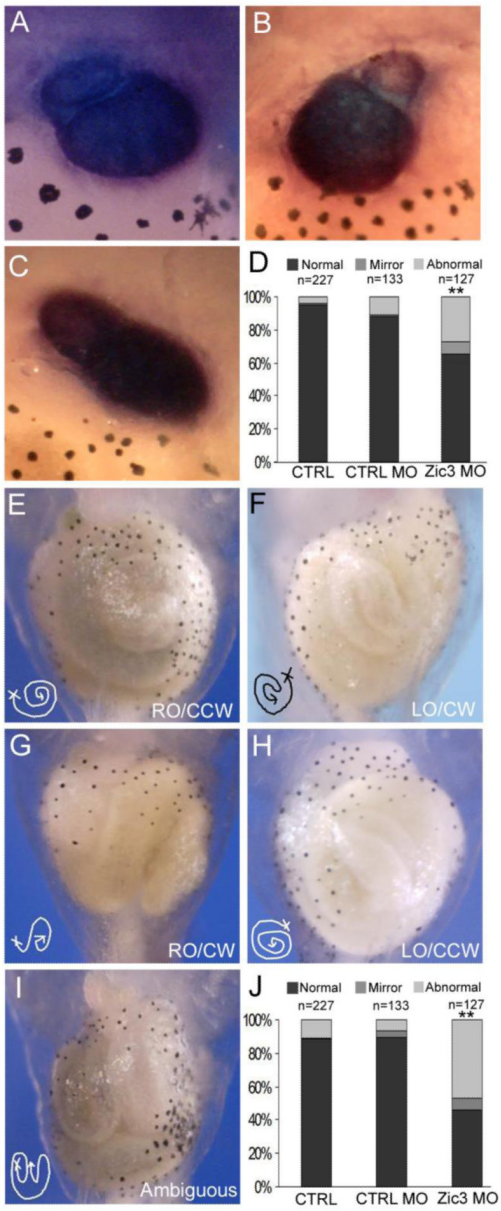

Fig. 5.

Reduction of *Zic3* expression results in heart and gut abnormalities. (A–C) Ventral view of *troponin* WISH staining of the heart in *Xenopus* stage 46 embryos. (A) Normal heart looping with outflow tract from the right side. (B) Mirror phenotype, with outflow tract from the left side. (C) Abnormal heart looping, with no clear laterality of the outflow tract position. (D) Quantification of heart looping phenotypes in controls and Zic3 morphants. (E–I) Ventral view of *Xenopus* gut coiling in control and Zic3 morphant stage 46 embryos. (E) Normal gut coiling, right origin (RO) and counter-clockwise coil (CCW) direction. (F) Mirror gut coiling phenotype, left origin (LO) and clockwise coil (CW) direction. (G) Normal gut origin with reversed coil direction, clockwise. (H) Mirror gut origin, left side, with normal coil direction, counter-clockwise. (I) Abnormal gut coiling phenotype, no clear origin or coil direction. (J) Quantification of gut coiling phenotypes in control and Zic3 morphants.

**$p<0.01$ by Fisher's exact test; statistical significance was determined through comparison of control morphants with Zic3 morphants.

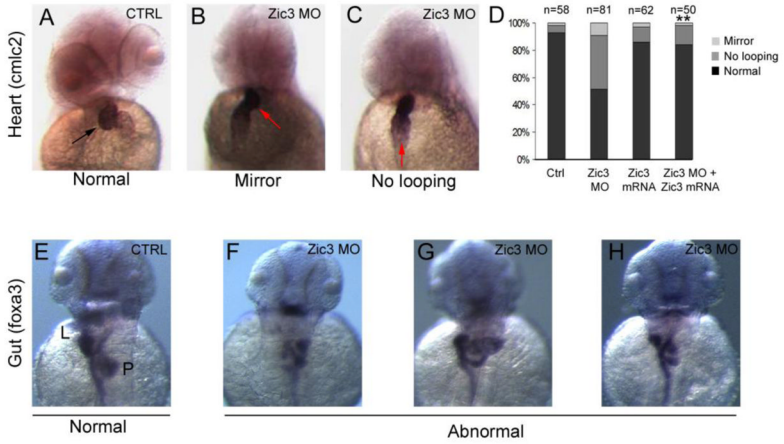

Fig. 6.

Abnormal heart looping and gut formation in zebrafish Zic3 morphants. (A–C) Direction of cardiac looping (arrows) visualized by WISH of *cardiac myosin light chain-2* (*cmlc2*) in 2 dpf embryos. Control embryos showed normal looping (A), whereas Zic3 morphants often showed mirror reversed (B) or unlooped (C) hearts. (D) Rescue of cardiac looping defects. Quantification of cardiac looping defects in control embryos is shown compared with embryos injected with Zic3 morpholino, *Xenopus zic3* mRNA, or co-injected with Zic3 morpholino and *Xenopus zic3* mRNA. (E–H) Analysis of gut looping by WISH with *foxa3* in 2 dpf embryos. Control embryos (E) showed normal asymmetric positioning of the liver (L) and pancreas (P). Organ position (F), patterning (G), and number (H) were abnormal in Zic3 morphants. $^{**}p<0.01$ by Fisher's exact test; statistical significance was determined through comparison of Zic3 MO + *zic3* mRNA with Zic3 MO to demonstrate phenotypic rescue.

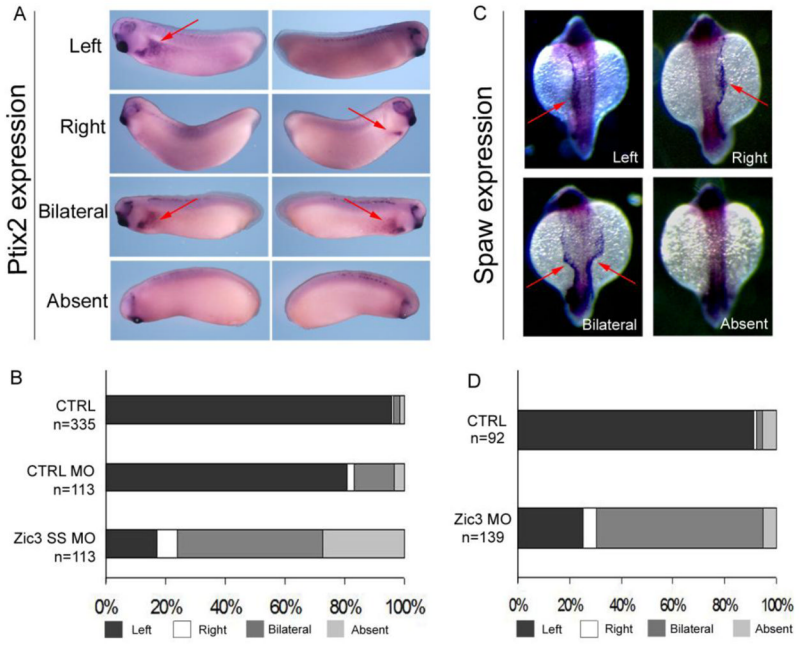

Fig. 7.

Abnormal L-R molecular marker expression in *Xenopus* and zebrafish Zic3 morphants. (A) *Pitx2* expression in *Xenopus* Zic3 morphant embryos at stage 30. Embryos were photographed from both left and right sides. Red arrows highlight *pitx2* expression. (B) Quantitative results of *pitx2* expression in non-injected control (CTRL), control morpholino (CTRL MO) and Zic3 splice site morpholino (SS MO). (C) *Southpaw* (*spaw*) expression in zebrafish Zic3 morphant embryos. Red arrows highlight gene expression as left, right, bilateral or absent. (D) Quantitative results of *spaw* expression in control and Zic3 morphants.

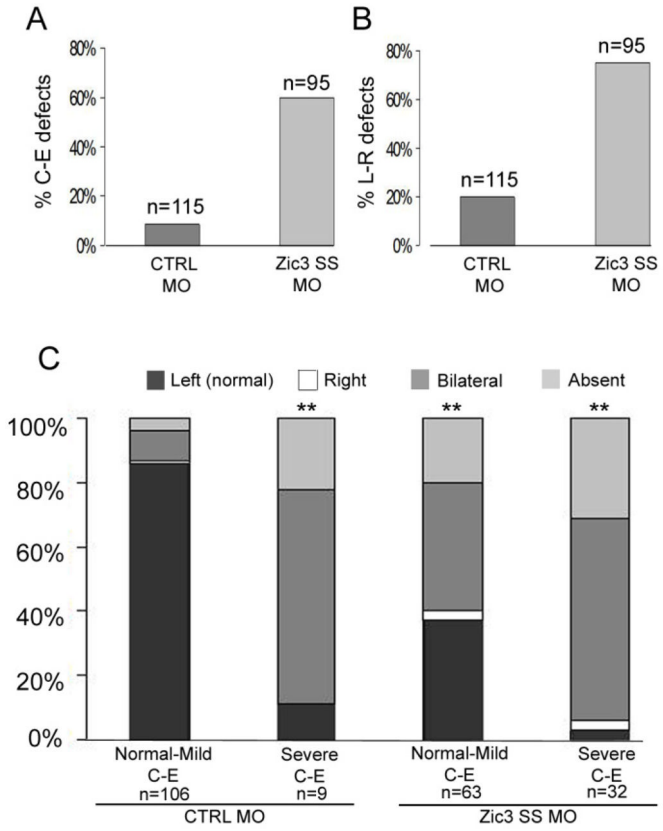

Fig. 8.

Correlation between C-E morphogenesis and L-R patterning. (A) Percentage of control morphant (CTRL MO) and Zic3 morphant embryos with defective C-E phenotypes. (B) Percentage of control and Zic3 morphants with L-R patterning abnormalities. (C) Comparison of control and Zic3 morphants with defective C-E (score based on scale represented in Fig. 1D) and abnormal L-R patterning (based on *pitx2* expression in the lateral plate mesoderm). C-E defects are categorized as normal to mild (C-E score of 1–3) and severe (C-E score of 4–5). ** $p<0.01$ by Fisher's exact test; statistical significance was determined through comparison of each experimental group with the CTRL MO (normal-mild CE) group.